Journal of Power Sources 195 (2010) 6329–6341

Contents lists available at ScienceDirect

Journal of Power Sources

journal homepage: www.elsevier.com/locate/jpowsour

Improving dynamic performance of proton-exchange membrane fuel cell system using time delay control

Young-Bae Kim*

Mechanical Engineering Department, Chonnam National University, Gwangju, Republic of Korea

ARTICLE INFO

Article history:
Received 28 January 2010
Received in revised form 29 March 2010
Accepted 6 April 2010
Available online 20 April 2010

Keywords:
Proton-exchange membrane fuel cell
Dynamical model
Compressor
Cooler
Anode recirculation
Time delay control

ABSTRACT

Transient behaviour is a key parameter for the vehicular application of proton-exchange membrane (PEM) fuel cell. The goal of this presentation is to construct better control technology to increase the dynamic performance of a PEM fuel cell. The PEM fuel cell model comprises a compressor, an injection pump, a humidifier, a cooler, inlet and outlet manifolds, and a membrane–electrode assembly. The model includes the dynamic states of current, voltage, relative humidity, stoichiometry of air and hydrogen, cathode and anode pressures, cathode and anode mass flow rates, and power. Anode recirculation is also included with the injection pump, as well as anode purging, for preventing anode flooding. A steady-state, isothermal analytical fuel cell model is constructed to analyze the mass transfer and water transportation in the membrane. In order to prevent the starvation of air and flooding in a PEM fuel cell, time delay control is suggested to regulate the optimum stoichiometry of oxygen and hydrogen, even when there are dynamical fluctuations of the required PEM fuel cell power. To prove the dynamical performance improvement of the present method, feed-forward control and Linear Quadratic Gaussian (LQG) control with a state estimator are compared. Matlab/Simulink simulation is performed to validate the proposed methodology to increase the dynamic performance of a PEM fuel cell system.

1. Introduction

Fuel cells provide environmentally friendly, high-efficiency power sources without the Carnot limitation of efficiency. The proton-exchange membrane fuel cell (PEMFC) is one of the most promising candidates for hybrid road vehicles by virtue of its high power density, zero pollution, low operating temperature, quick start-up capability, and long life.

There are three major subsystems in a typical pure hydrogen fuel cell system, namely: air supply, fuel supply and recirculation, and water and thermal management (including humidification and purge.) Flow rates and pressures are controlled to avoid oxygen starvation, water flooding of the membrane, and excessive auxiliary power consumption by the air supply subsystem. Anode recirculation is used to reduce hydrogen waste, maintain a pressure difference between anode and cathode minimal, and run the fuel in the anode to obtain better water management. The dynamic response of the fuel cell system is important for vehicular applications where power demand fluctuates and where the fuel cell and other subsystems do not usually operate at the optimum steady-states designed by the manufacturer. Therefore, constructing a precise PEM fuel cell dynamical model is crucial, in addition to adopting a robust control technique, to meet the power fluctuation requirements.

A number of fuel cell models have been devised to predict polarization [1–5]. While providing good understanding of the fuel cell fundamentals, these contributions at the cell level are not suitable for the study of control. Compared with these steady-state studies, few dynamic models of fuel cell systems have been published [6–11]. Pukrushpan et al. [12] developed a system-level model that included a compressor, a supply and return manifolds, humidifier, and anode and cathode channels. This model is used for the air system control without including anode recirculation. He used linear quadratic regulation (LQR) optimal control theory to increase the transient performance; however, the control requires an observer and lengthy linearization process, and only regulation of the oxygen ratio was discussed in the study. The linear model has also been used; however, it is not sufficient for application in the nonlinear PEMFC model. In addition to the linear analysis, increasingly adaptive and intelligent controllers have been designed for fuel cell application. Schumacher et al. [13] presented a fuzzy logic controller for a miniature PEMFC. Hasikos et al. [14] applied a neural network in the robust control of hydrogen utilization with oxygen stoichiometry regulation. Shen et al. [15] designed an adaptive fuzzy controller for temperature control in a molten carbonate fuel cell (MCFC) stack. Model-predictive control has also been used for the power tracking of a fuel cell [16]. Most studies have focused on airflow control, temperature control, or power optimization. Bao et

* Tel.: +82 62 530 1677; fax: +82 62 530 1689.
E-mail address: ybkim@chonnam.ac.kr.

0378-7753/$ – see front matter © 2010 Elsevier B.V. All rights reserved.
doi:10.1016/j.jpowsour.2010.04.042

Nomenclature

A	system matrix or area (m^2)
B	constant or state matrix
B^+	pseudo-inverse of B matrix
$\hat{B}$	estimation of B matrix
C	concentration or state matrix
d	disturbance
D	state matrix
e	error vector
E_{Nernst}	Nernst instantaneous voltage (V)
f	non-linear function
$\hat{f}$	estimation of function f
F	feedback gain matrix or Faraday constant ($C\,mol^{-1}$)
h	unknown disturbance vector
I	current (A)
J	current density ($A\,m^{-2}$) or performance index or rotational inertia ($kg\,m^2$)
k	nozzle constant
K	gain matrix
L	time delay (s)
m	mass (kg)
M	molar mass ($kg\,mol^{-1}$)
n	number of cells
N	number of poles
P	pressure (Pa)
q	molar flow ($mol\,s^{-1}$) or converted mass flow rate in the injection pump ($m^3\,s^{-1}$)
Q	weighting matrix
r_m	resistivity ($\Omega\,m$)
R	weighting matrix
R_C	contact resistance (Ω)
R_{comp}	compressor resistance (Ω)
R_m	equivalent membrane impedance (Ω)
R_{ohmic}	internal ohmic resistance (Ω)
t	Time (s)
T	Temperature (K)
T_s	sampling time (s)
u	control input or injection coefficient
V or v	voltage (V)
V_{act}	activation overvoltage (V)
V_{conc}	concentration overvoltage (V)
V_{ohmic}	ohmic overvoltage (V)
w	noise variable
W	mass flow rate ($kg\,s^{-1}$)
x	state variable or state vector
$\dot{x}$	state vector derivative with time
y	control output
$\hat{y}$	observer output
z	performance or observer state matrix

Greek symbols

γ	specific heat ratio
δ	water content of the membrane
ε	relative density
ζ	constants utilized in modeling of activation voltage
η	efficiency
λ	converted adiabatic velocity ($m\,s^{-1}$) or stoichiometry
ξ	damping ratio
Π	pressure ratio
ρ	density ($kg\,m^{-3}$)
τ	torque ($N\,m^{-1}$)
φ	velocity correction coefficient
Φ	magnetic flux (Wb)
ϕ	relative humidity
ω	angular velocity ($rad\,s^{-1}$)
ω_n	natural frequency (s^{-1})

Superscripts and subscripts

a	air
an	anode
atm	atmosphere
C	compressed flow in the injection pump
ca	cathode
comp	compressor
cooler	cooler
diff	difference
e	error
fc	fuel cell stack
gen	generation
H	pumped flow in the injection pump
H_2	hydrogen
humid	humidifier
im	inlet manifold
in	inlet
l	liquid
m	model reference
memb	membrane
N_2	nitrogen
nozzle	nozzle
O_2	oxygen
om	outlet manifold
out	outlet
P	pumping flow in the injection pump
PH	ratio between pumping flow and pumped flow
pump	injection pump
purge	purge
react	reaction
recircle	recirculation
sat	saturation
T	transpose
*	target value

al. [17] developed multiple input–output controllers for increasing transient PEM fuel cell dynamic response. Model-predictive control was suggested for the non-linear PEM fuel cell model; however, prolonged training of the neural model is required to render the method practical. Moreover, fuzzy or neural controllers are based on the linear model and disturbance or time varying parameters such as change in temperature cannot be eliminated effectively. There are currently only a few reports that pertain to robust PEMFC control.

Compared with the above use of fuzzy or LQR controls to regulate oxygen and hydrogen stoichiometry, this investigation focuses on improving the transient behaviour of a PEMFC by applying the robust control method. As the problem of regulating oxygen and hydrogen stoichiometry requires encompassing modeling uncertainty or variation of PEMFC system parameters due to variations in the operating environment, a more robust or variation-free control technique is essential. A method used to meet the above conditions is time delay control (TDC) [18–20]. This technique can render the state variables to follow accurately the reference dynamics by utilizing plant input and output information within a few sampling periods. It can adapt the control input into the reference dynamics even with varying plant parameters or disturbance to the system. The TDC technique does not require gain-phase adjustments nor

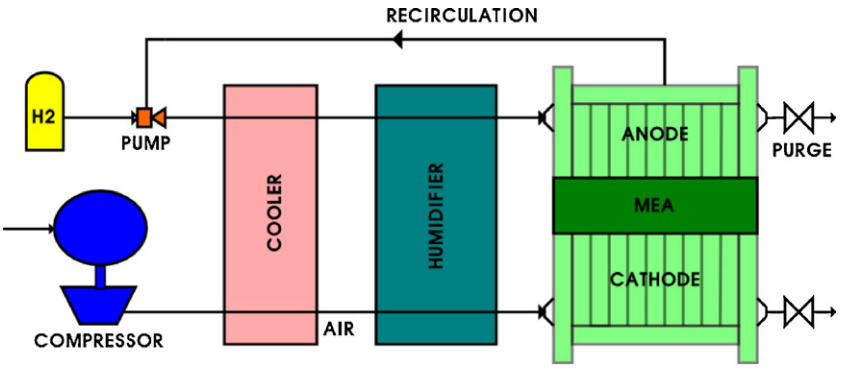

Fig. 1. Configuration of PEM fuel cell system.

does it track the control variable in the manner of most control algorithms. Since the job of non-linear PEMFC dynamic model identifying in real-time basis is not necessary in TDC, its logic is simpler and more compact in comparison with other control algorithms. Furthermore, it has the advantage of an available controller design, even when the exact PEMFC dynamics are not ready or when the model dynamics error cannot affect control performance.

2. Fuel cell system model

A diagram of the air supply system, hydrogen supply and recirculation subsystem in a PEMFC is shown in Fig. 1. This is the prototype of a high-pressure fuel cell system (FCS) (80 kW stack) in a Korean fuel cell hybrid sports utility vehicle (SUV) [21]. A compressor driven by a motor is used to obtain the proper airflow. At the end of the outlet manifold in the cathode, a proportional back-pressure valve enables regulation of the cathode pressure. In the anode loop, an injection pump enables anode recirculation. The characteristics of the injection pump can be changed by regulating the pressure of the pumping flow with a proportional pressure regulator. At the end of the anode outlet is a purge valve. As shown in Fig. 1, the filled blocks, including the compressor, cathode inlet and outlet manifolds, and lumped anode and cathode volumes, dominate transient behaviour. Considering the relatively small volume of anode inlet and outlet manifolds and the small pressure drop in the anode loop, all volumes are combined into one lumped volume. Since the temperature of the air leaving the compressor is very high, a cooler is necessary to decrease the inlet temperature of the membrane. The study assumes that the membrane electrode assembly (MEA) temperature is 80 °C, which has been observed in most PEMFCs. A steady-state, isothermal analytical fuel cell model is also adopted to analyze the mass transfer and water transportation in the membrane. A dynamical PEMFC model is justified because thermal dynamic behaviour has slower dynamics compared with mass flow or water transportation dynamics. As the temperature fluctuation in most MEAs is 4 °C [22], the thermal effect can be ignored.

2.1. PEM fuel cell stack

Most fuel cell models that describe the physical behaviour of a PEMFC are represented either by empirical equations fitted to the curve of the polarization characteristics or by computational fluid dynamics (CFD) to solve the transport of mass and charges. The former can be used to describe a steady-state behaviour but lacks the full dynamics that are complemented by reflecting the double-layer capacitor [23]. These models do not provide the gas dynamics dominant along the flow paths.

CFD-based models have been widely employed to analyze physical phenomena in a single cell; however, they are limited to representing dynamic characteristics in conjunction with components of the balance-of-plant (BOP) used for the analysis of power system. Consequently, a dynamical model is necessary. Thus, the present study includes water balance in the membrane and BOP characteristics.

A cell is constructed by individual model layers. Of these layers, three obtain a current–voltage static relationship in a cell: the ohmic overpotential in the membrane, the activation overpotential in the catalyst on the cathode side, and the concentration overpotential. The voltage drop for a cell is dependent on the reactant partial pressure and membrane water content [24], i.e.,

$$V_{fc} = E_{Nernst} - V_{act} - V_{conc} - V_{ohmic} \quad (1)$$

The Nernst's instantaneous voltage can be written as [1]

$$E_{Nernst} = 1.229 - (8.5 \times 10^{-4})T - 298.15 + 4.308 \times 10^{-4} \times T \times \ln(P_{H_2} + 0.5P_{O_2}) \quad (2)$$

The molar flow of hydrogen that reacts in order to meet the load change can be found as

$$q_{H_2} = \frac{I_{fc}}{2F \times A_{fc}} \quad (3)$$

The following expression gives the activation overvoltage occurring in a PEMFC system [4]:

$$V_{act} = \xi_1 + \xi_2 T + \xi_3 T(\ln(I_{fc})) + \xi_4(\ln C_{O_2}) \quad (4)$$

In Eq. (4), the concentration of dissolved oxygen at the gas/liquid interface can be defined by a Henry's law expression of the form:

$$C_{O_2} = \frac{P_{O_2}}{5.08 \times 10^6 \exp(-\frac{498}{T})} \quad (5)$$

Ohmic overvoltage in fuel cell system is the measure of the $I \times V$ voltage drop associated with the proton conductivity of the polymer electrolyte and electronic internal resistances. Thus, the ohmic overvoltage in a fuel cell can be represented as:

$$R_m = I_{fc} \times R_{ohmic} = I_{fc} \times (R_m + R_C) \quad (6)$$

The equivalent membrane impedance can be expressed in Ohm's law as:

$$R_m = \frac{r_m \times l}{A_{fc}} \quad (7)$$

The resistivity of a Nafion type of proton-exchange membrane can be calculated from Eq. (7) as [25]:

$$r_m = \frac{181.6[1 + 0.03\ J + 0.062 \times \left(\frac{T}{303}\right)^2 \times J^{2.5}}{[\delta - 0.634 - 3\ J] \exp\left[4.18 \times \left(T - \frac{303}{T}\right)\right]} \quad (8)$$

The concentration overvoltage can be expressed as:

$$V_{\text{conc}} = B \times \ln\left(1 - \frac{J}{J_{\max}}\right) \tag{9}$$

Finally, the voltage of a fuel cell stack formed by n cells connected in is given by:

$$V_{\text{stack}} = n \times V_{\text{fc}} \tag{10}$$

2.2. Air flow system

The air supply system consists of a compressor, cooler, humidifier, and manifolds for the inlet and outlet. The outlet of a compressor driven by an electric motor is connected to the cooler, humidifier, and an inlet of flow channels through pipes. In this study, the humidifier is simplified into an ideal one without any associated dynamics and energy losses.

The compressor is constructed with an impeller driven by an electric motor. The dynamic response of the blower is described by the inertia of the motor and impeller, and the torque produced by the motor. Hence, the torque produced by the motor, τ_{comp}, is a function of the stator resistance, R_{comp}, the magnetic flux constant, Φ_{comp}, and the number of the poles, N_{comp}, with the stator voltage v_{comp}. Therefore, the flow rate (W_{comp}) can be controlled by the voltage of the motor, v_{comp} [22], i.e.,

$$\frac{d\omega_{\text{comp}}}{dt} = \frac{1}{J_{\text{comp}}}\left(\tau_{\text{comp}} - \frac{W_{\text{comp}}\Delta p_{\text{comp}}\eta_{\text{comp}}}{\eta_{\text{comp}}\rho_{\text{amb}}\omega_{\text{comp}}}\right) \tag{11}$$

$$\tau'_{\text{comp}} = \eta_{\text{comp}}\frac{3}{2}\left(\frac{N_{\text{comp}}p_{\text{comp}}}{2}\right)\left(\frac{\Phi_{\text{comp}}}{R_{\text{comp}}}\right) \tag{12}$$

$$\tau_{\text{comp}} = \left[v_{\text{comp}} - \left(\frac{N_{\text{comp}}}{2}\right)\Phi_{\text{comp}}\omega_{\text{comp}}\right] \times \tau'_{\text{comp}} \tag{13}$$

The parameters for the compressor are derived by characteristic data and specifications, which usually include both flow parameter and overall efficiency versus the head parameter [26]. The relation between compressor speed, downstream pressure, and compressor airflow rate is governed by the compressor flow map.

The compressed airflow enters through the inlet manifold and influences the changes in the pressure inside the inlet manifold through mass and energy conservation laws.

$$\frac{dm_{\text{im}}}{dt} = W_{\text{comp}} - W_{\text{in,out}} \tag{14}$$

$$\frac{dm_{\text{im}}}{dt} = \frac{\gamma Ra}{V_{\text{im}}}\left(W_{\text{comp}}T_{\text{comp}} - W_{\text{in,out}}T_{\text{im}}\right) \tag{15}$$

The change in inlet manifold pressure affects the rate of air entering the stack cathode through the linear nozzle equation, where k_{im} is the inlet manifold nozzle constant.

$$W_{\text{im}} = K_{\text{im}}(p_{\text{im}} - p_{\text{ca}}) \tag{16}$$

The temperature of the air in the inlet manifold is typically higher due to the high temperature of air leaving the compressor (over 100 °C), which degrades the fuel cell performance [21]. To prevent further malfunction to the fuel cell membrane, the air needs to be cooled down to the stack operating temperature. In this study, an ideal cooler is assumed to keep the temperature of the air entering the stack at $T_{\text{cooler}} = 80\,^{\circ}\text{C}$. It is also assumed that there is no pressure drop in the cooler. As temperature change effects gas humidity the relative humidity of the gas exiting the cooler is obtained as:

$$\phi_{\text{cooler}} = \frac{p_{\text{cooler}}\phi_{\text{atm}}p_{\text{sat}}(T_{\text{atm}})}{p_{\text{atm}}p_{\text{sat}}(t_{\text{cooler}})} \tag{17}$$

where $\phi_{\text{atm}} = 0.5$ is the assumed ambient air relative humidity and $p_{\text{sat}}(T_i)$ is the vapour saturation pressure at a gas temperature T_i.

Airflow from the cooler should be humidified before entering the stack since the cooler condenses vapour to lower the relative humidity. A static model of the humidifier is used to calculate the change in air humidity. The temperature of the airflow is assumed to be constant. Based on the condition of the flow exiting the cooler, the vapour pressure is determined by:

$$p_{v,\text{cooler}} = \phi_{\text{cooler}}p_{\text{sat}}(T_{\text{cooler}}) \tag{18}$$

The vapour pressure can be calculated as:

$$p_{v,\text{humid}} = \frac{W_{v,\text{humid}}M_a}{W_{a,\text{cooler}}M_v}p_{a,\text{cooler}} \tag{19}$$

The humidifier exit flow relative humidity can be obtained as:

$$\phi_{\text{humid}} = \frac{p_{v,\text{humid}}}{p_{\text{sat}}(T_{\text{cooler}})} \tag{20}$$

The humidity exit flow rate is governed by the mass continuity:

$$W_{\text{humid}} = W_{a,\text{cooler}} + W_{v,\text{humid}} \tag{21}$$

As the flow leaving the humidifier enters the fuel cell cathode, it is referred to as cathode inlet flow. The rate of this air flow into the cathode affects the oxygen level in the cathode and thereby affects both stack voltage and stack power output. The dynamics of the oxygen level in the cathode is governed by the mass conservation law. There are three states in the cathode volume model: the oxygen mass $m_{\text{O}_2\text{ca}}$, the nitrogen mass $m_{\text{N}_2\text{ca}}$ and the vapour mass $m_{v\text{ca}}$. Their state equations are:

$$\frac{dm_{\text{O}_2\text{ca}}}{dt} = W_{\text{O}_2\text{ca,in}} - W_{\text{O}_2\text{ca,out}} - W_{\text{O}_2,\text{react}} \tag{22}$$

$$\frac{dm_{\text{Nca}}}{dt} = W_{\text{N}_2\text{ca,in}} - W_{\text{N}_2\text{ca,out}} \tag{23}$$

$$\frac{dm_{v\text{ca}}}{dt} = W_{v\text{ca,in}} - W_{v\text{ca,out}} + W_{v\text{ca,gen}} + W_{v,\text{memb}} - W_{\text{l,caout}} \tag{24}$$

The oxygen partial pressure which affects the stack voltage can be calculated from these states using the ideal gas law. The amount of oxygen reacted or used in the reaction, $W_{\text{O}_2,\text{react}}$, is a function of the stack current I_{fc}, which is considered as the disturbance input.

$$W_{\text{O}_2,\text{react}} = M_{\text{O}_2}\frac{nI_{\text{fc}}}{4F} \tag{25}$$

The function in the linear nozzle equation is in the same form as Eq. (16), where $k_{\text{om,out}}$ is the outlet manifold nozzle constant, and p_{ca} and p_{om} are the cathode and the outlet manifold pressure, respectively. In this study, p_{om} is assumed to be 1 atm.

$$W_{\text{om,out}} = k_{\text{om,out}}(p_{\text{ca}} - p_{\text{om}}) \tag{26}$$

From the above equations, the electrical current drawn from the stack will cause the oxygen partial pressure to drop inside the cathode volume. This reduces the stack efficiency and increases the risk of oxygen starvation. To replenish the oxygen, the compressor has to increase the airflow to the inlet manifold. But, the cathode oxygen cannot be replenished instantaneously since the dynamics of the compressor, inlet manifold and cathode volume are affected. The outlet manifold valve opening can be used to alter the cathode oxygen transient response by closing it down or opening up during transients.

2.3. Hydrogen flow system

The anode flow system is different from the cathode flow system since the hydrogen is delivered through an injection pump with an expansion section. In this study, hydrogen is supplied to the anode of the fuel cell through a hydrogen tank. The pumping flow rate can be instantaneously adjusted through a valve to maintain the minimum pressure difference between the cathode and the

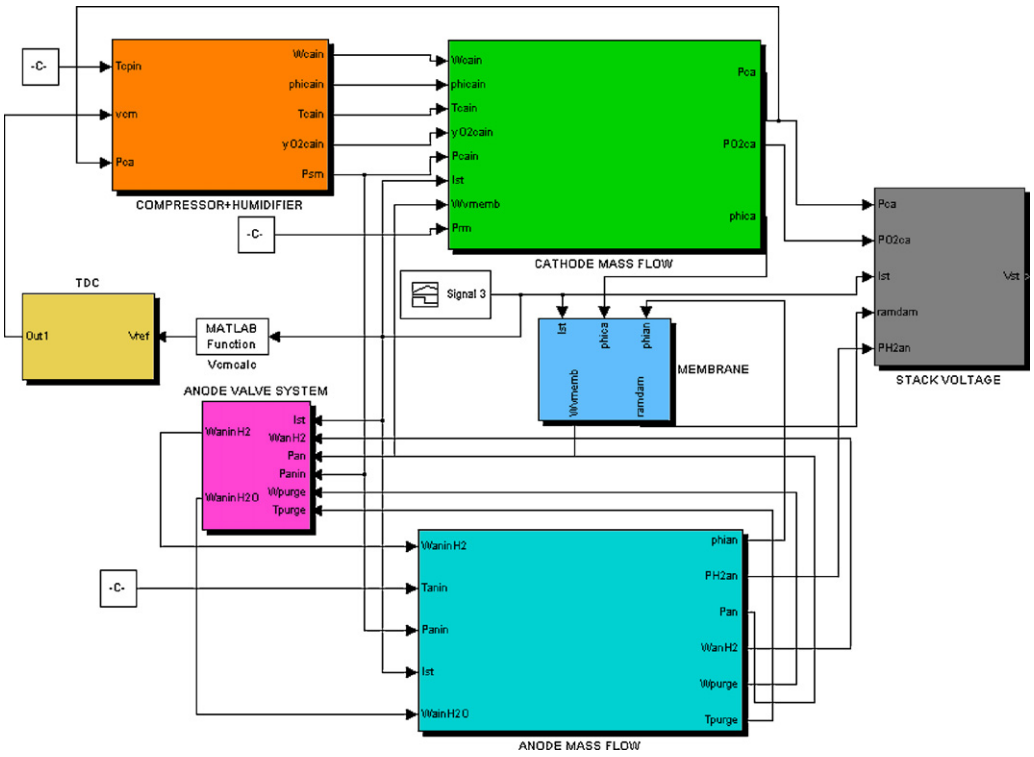

Fig. 2. Matlab/Simulink model of PEM fuel cell system.

anode. Hydrogen recirculation is also utilized to reduce hydrogen usage. While pumping flow crosses via a nozzle, the pumped flow is inhaled into the receiving chamber. During the mix of the pumping flow and the pumped flow, energy and momentum are exchanged and result in a compressed flow in the mixing chamber. Since the pressure difference between the pumping flow and pumped flow in the anode recirculation loop is small, the non-linear relationship in the following equation can be obtained through the conservation of mass and energy momentum theorem [27].

$$\frac{P_C - P_H}{P_H} = k\Pi_{P*}\frac{P_P f_{P1}}{P_H f_{P3}} q_{PH}^2 \times \left[\varepsilon_{P*}(\varphi_2\varphi_4 - 0.5)\frac{\rho_P}{\rho_H}\frac{f_{P1}}{f_3 - f_{P1}}u^2 + \varphi_1\varphi_3\frac{\lambda_{PH}}{q_{PH}}\right] - \varepsilon_{P*}\left(\frac{1}{\varphi_4} - 0.5\right)\frac{\rho_P}{\rho_C}\frac{f_{P1}}{f_3}(1+u)^2 \quad (27)$$

The above equation can be simplified as:

$$W_{an,pump} = \begin{cases} k_{an,pump}(p_{ca} - p_{an}) & \text{if } p_{ca} \geq p_{an} \\ k_{an,recircle}(p_{an} - p_{ca}) & \text{if } p_{ca} < p_{an} \end{cases} \quad (28)$$

where $k_{an,pump}$ and $k_{an,recircle}$ are the nozzle coefficient from pumping flow into the anode section and the coefficient from pumped flow into the anode, respectively. The hydrogen is usually supplied from the injection pump into the anode; however, if the anode pressure is larger than that of the cathode pressure, then recirculation begins.

Impurities gradually accumulate in the cells near the fuel exhaust outlet. Proper management is required to provide enough hydrogen fuel for these particular anodes to perform the electrochemical reaction. Periodical purging or continuous exhaust release is required for diluting or refreshing the exhaust build-up, although a stack may be claimed as a dead-end structure. In this study, periodical purging is adopted to release accumulated water or impurities, including hydrogen. For the purge analysis, the following equation can be used:

$$W_{an,purge} = k_{an,purge}(p_{an} - p_{atm}) \quad (29)$$

Similar to the cathode flow model, hydrogen partial pressure and anode flow humidity are determined by balancing the mass flow of hydrogen and vapour in the anode.

$$\frac{dm_{H_2an}}{dt} = W_{H_2an,in} - W_{H_2an,out} - W_{H_2,react} \quad (30)$$

$$\frac{dm_{vca}}{dt} = W_{van,in} - W_{van,out} - W_{v,memb} - W_{l,an,out} \quad (31)$$

In above equation, the following equations are used:

$$W_{H_2an,out} = W_{an,purge} \quad (32)$$

$$W_{H_2an,in} = W_{an,pump} \quad (33)$$

The configuration diagram for the PEMFC model constructed with Matlab/Simulink is given in Fig. 2. Experimental validation for the model can be referred to in Ref. [11].

3. Flow control

The focus of the air supply system in a FCS is to avoid oxygen starvation and to respond to the immediate power demand requirement. Corresponding to a specific electrode load, the excessive amount of reactant is described by the stoichiometric ratio, which is the ratio of the reactant supplied to the reactant used. As the dominant consumer of auxiliary power, the compressor is the only parasitic unit described in this study. With increasing air stoichiometric ratio and corresponding pressure, the stack gross power improves and the compressor consumption increases. This trade-off and the steady-state optimum operation conditions have been analyzed in detail [28]. As the net power increases, the optimum pressure continually rises and the optimum air stoichiometric ratio shows a non-monotonous trend. Here, the desired air stoichiome-

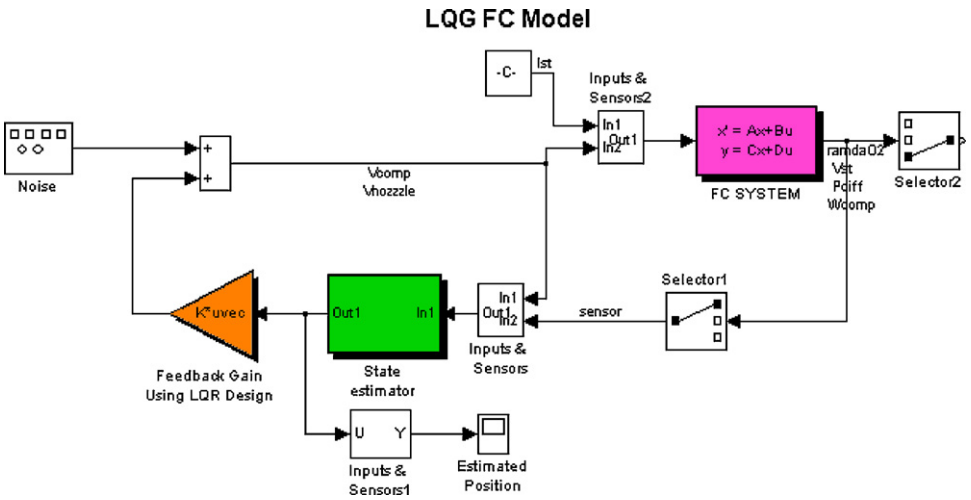

Fig. 3. Matlab/Simulink model of LQG controller.

try is chosen to be constant (air stoichiometry = 2), which has been found to yield maximum fuel cell power [12].

In addition to avoiding fuel waste and humidifying the hydrogen, maintaining the pressure difference between the anode and cathode is another task for the fuel supply and recirculation subsystem because frequent changes in pressure difference will damage the membrane.

The control problem for the highly non-linear model is to obtain good transient and steady performance. This must include optimum air stoichiometry and no pressure difference between the anode the cathode.

3.1. Feedfoward control

In order to achieve the above objectives, static feedfoward (FF) control can be used to achieve the desired operation. The target dry air flow rate can be obtained by:

$$W_{\text{compressor}} = \frac{\lambda_{O_2} I_{\text{fc}} n M_a}{4F(0.21)} \tag{34}$$

$$W_{\text{pump}} = \frac{\lambda_{H_2} I_{\text{fc}} n M_{H_2}}{2F} \tag{35}$$

The control input of the compressor motor, v_{comp}, can be obtained from the power balance between the compressor and the motor. The FF controller is obtained by simulating various operating conditions. After interpolating the input voltage of v_{comp}, v_{nozzle}, which satisfies the Eqs. (34) and (35), the final FF controller is obtained. This is an easy and rapid calculation process with several simulations; however, it has a disadvantage in that its transient response shows poor performance in regulating the desired parameters because it is an open-loop system. The advantage of the FF controller is that it is easy to implement and covers the fuel cell system with certain level of non-linearity.

3.2. LQG control with Kalman estimator

The dynamic non-linear model for air stream, hydrogen flow with recirculation, and anode purging in a PEMFC system is described as:

$$\dot{x} = f(x, u, w), \quad u = [v_{\text{comp}}, v_{\text{nozzle}}]^T \tag{36}$$

$$w = I_{\text{fc}} \tag{37}$$

$$x = [\omega_{\text{comp}}, m_{O_2}, m_{N_2}, m_{v\text{ap,ca}}, m_{H_2}, P_{\text{ca}}]^T \tag{38}$$

$$z = [\lambda_{O_2}, P_{\text{diff}}]^T \tag{39}$$

$$y = [v_{\text{fc}}, W_{\text{comp}}]^T \tag{40}$$

The purpose of the LQG controller is to track the control inputs under the disturbance of change in stack current. The controller should also preserve the desired oxygen stoichiometry and transform the pressure difference between cathode and anode to zero. As the outputs of stack voltage, v_{fc}, and compressor flow rate, W_{comp}, are easily measured, their values are directly fed back by the LQG gain K from the Matlab control toolbox, i.e.,

$$K = lqr(A, B, C^T, Q, C, R) \tag{41}$$

$$J = \int_0^\infty (\delta Z^T Q \delta Z + \delta u^T R \delta u) dt \tag{42}$$

In the above equations, the oxygen stoichiometry tracking value is 2, and the pressure difference between the anode and the cathode is set to zero. The state matrices A, B, C and D are obtained using linearized operating conditions with I_{fc} = 300 A, v_{comp} = 130 V, and v_{nozzle} = 128 V. Since the oxygen stoichiometry is difficult to measure, an estimated value is obtained using a Kalman filter and fed back into the inputs of v_{comp},v_{nozzle}. The Simulink LQG control diagram for the PEMFC model is shown in Fig. 3. The inputs and outputs can be selected through port selectors. Since the model is inherently linear (i.e., obtained from one of the operating points of the PEMFC) it is difficult to use in satisfying all the operating conditions. Therefore, a non-linear PEMFC model is necessary to regulate the oxygen stoichiometry constant and the pressure difference between the anode and the cathode zero. On the other hand, building the non-linear model is a lengthy and therefore time-consuming process [17]; thus, a robust control method that is also easy to implement in a real-time environment and applicable to the non-linear dynamical system is necessary.

3.3. Time delay control

All state variables and their derivatives are assumed to be observable and the non-linear time invariant plant can be expressed as

$$\dot{x} = f(x, t) + h(x, t) + B(x, t)u + d \tag{43}$$

The matrix $B(x,t)$ is assumed to be known. The purpose of TDC is to design a controller to obtain the required performance under unknown environments. Therefore, the required performance is

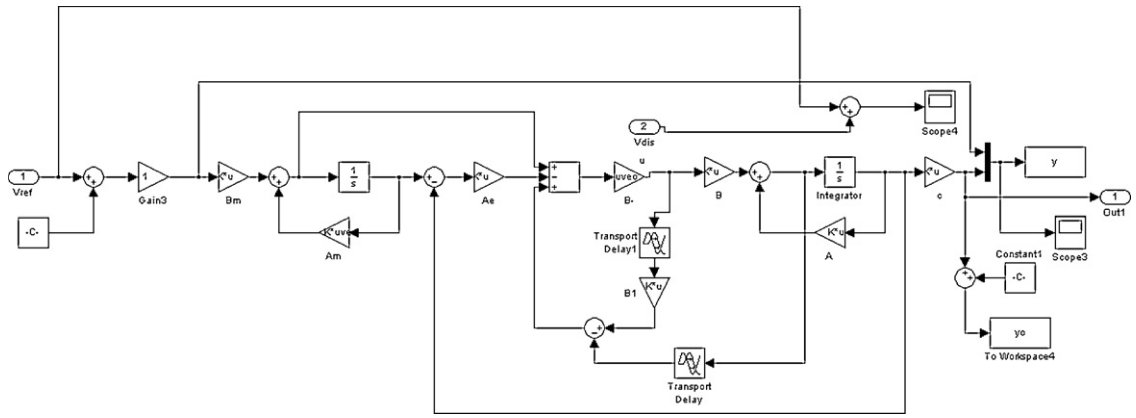

Fig. 4. Matlab/Simulink model of TDC controller.

defined as the reference model as:

$$\dot{x}_m = A_m x_m + B_m r \tag{44}$$

If e is defined as an error vector between x_m and x, then the desired error dynamic becomes:

$$\dot{e} = A_e e \tag{45}$$

If all the eigenvalues of A_e locate on the left half plane, then the errors will become null as time passes, therefore, the errors will be asymptotically stable. Using the above equations, the following equation can be obtained:

$$B(x,t)u = -f(x,t) - h(x,t) - d + \dot{x}_m - A_e e \tag{46}$$

As the inverse of $B(x,t)$ exists always, and if the pseudo-inverse of B is defined as $B^+ = (B^T B)^{-1} B^T$, then an approximated solution of $u(t)$ can be obtained as:

$$u = B^+(x,t)\{-f(x,t) - h(x,t) - d + \dot{x}_m - A_e\} \tag{47}$$

In order to determine whether u as defined by the above expression could satisfy the error dynamics of Eq. (45), Eq. (47) is inserted into Eq. (46). This results in the following error dynamics equation with a constrained equation:

$$\dot{e} = (A_m + K)e + (I - \hat{B}\hat{B}^+)[-\hat{f}(x,t) + A_m x + B_m r - Ke] \times (I - \hat{B}\hat{B}^+) \tag{48}$$

$$[-\hat{f}(x,t) + A_m x + B_m r - Ke] = 0 \tag{49}$$

If the constrained Eq. (49) is satisfied, and the eigenvalues of $(A_m + K)$ locate on the left half plane, then the error of Eq. (48) will converge to zero.

3.3.1. Compensator design

The input values of the plant represented by Eq. (47) can be specified under the condition that the unknown function of $h(x,t) + d(t)$ should be pre-defined. If the unknown function $h(x,t) + d$ is a continuous one and the time delay L is small enough, then the difference between $h(x,t) + d$ and $h(x(t-L),t-L) + d(t-L)$ is minimal, that is:

$$\begin{aligned}\hat{h}(x,t) + \hat{d} &\approx h(x(t-L),t-L) + d(t-L) \\ &= \dot{x}(t-L) - f(x(t-L),t-L) - B(x(t-L),t-L)u(t-L)\end{aligned} \tag{50}$$

Therefore, unknown estimated values are obtained from the previous measurement value, state variables, and control input information.

In most cases, the matrix of $B(x,t)$ is always unknown or uncertain, therefore, $\hat{B}$, which is the estimation of $B(x,t)$, is used. The following equation can be then be derived from Eqs. (47) and (50).

$$u = \hat{B}^+\{-f(x,t) - \dot{x}(t-L) + f(x(t-L),t-L) + \hat{B}(t-L)u(t-L) \tag{51}$$

The control input of Eq. (51) can be described simply by placing the sampling time T_s equal to L or multiplying the integer for the purpose of easy calculation. A more careful decision of the T_s can be referenced [29].

3.3.2. Observer design

In the above TDC expressions, all state variables are assumed to be observable. In a real feedback control problem, however, not all the variables are measurable. Therefore, it is compulsory to design an observer that can be interfaced with TDC, such as the Leuenberger observer for accurate control. For the unknown non-linear system, the unknown uncertainty and state variables should be observed. As a reference model is introduced in the present system, the following simplified linear observer can be utilized:

$$\dot{z} = A_m z + B_m r + F(y - \hat{y}) = A_m z + B_m r + FC(z - x) \tag{52}$$

where z and $\hat{y}$ are the observer state variable and the observer output, respectively. The reference model dynamics is used by the above-observed model, because the plant dynamics of Eq. (43) follow the reference dynamics under the application of TDC. The observed variable z is utilized instead of the state variable x, and the time delayed estimation of the unknown dynamics $h(x,t) + d$ is accomplished by variable z. Therefore, the control input u is determined as:

$$u = \hat{B}^+\{-f(z,t) - h(z,t) - d + \dot{x}_m - A_e e\} \tag{53}$$

$$h(x,t) + d = \dot{z}(t-L) - f(z(t-L),t-L) - \hat{B}(t-L)u(t-L) \tag{54}$$

The objective of the time delay controller is to render accurately the control output to follow the reference model output, although some output disturbances or parameter changes might exist. In doing so, the reference model is designed to have asymptotical stable roots. Since the compressor plant dynamics are represented approximately by third order [30], the reference model is designed to have:

$$\frac{X_m(S)}{R(S)} = \frac{5\zeta\omega_n^3}{(s^2 + 2\zeta\omega_n s + \omega_n^2)(s + 5\zeta\omega_n)} \tag{55}$$

The steady-state form of the reference model has the following form:

$$A_m = \begin{bmatrix} 0 & 0 & 0 \\ 0 & 0 & 1 \\ -5\zeta\omega_n^3 & -10(\zeta^2\omega_n^2 + \omega_n^2) & -7\zeta\omega_n \end{bmatrix} \tag{56}$$

$$B_{\mathrm{m}} = \begin{bmatrix} 0 \\ 0 \\ 5\zeta\omega_n^3 \end{bmatrix} \tag{57}$$

The steady-state form of the error matrix is represented as:

$$A_{\mathrm{g}} = \begin{bmatrix} 0 & 1 & 0 \\ 0 & 0 & 1 \\ -5\zeta\omega_n^3 & -10(\zeta^2\omega_n^2 + \omega_n^2) & -7\zeta\omega_n \end{bmatrix} \tag{58}$$

In the TDC design, it is very important to obtain the estimated value of $\hat{B}$ and the pseudo-inverse of $\hat{B}^{+}$. They are expressed as

$$\hat{B} = [0.1429 \;\; 0.5285 \;\; 1.0591]^T \tag{59}$$

$$\hat{B}^{+} = (B^T B)^{-1} B^T = [0.1005 \;\; 0.3718 \;\; 0.7451]^T \tag{60}$$

The simulink block diagram for TDC in the present study is given in Fig. 4.

4. Simulation results and analysis

The step input response of oxygen stoichiometry, both with and without LQG controllers is shown in Fig. 5. As shown in the figures, the LQG controller with a Kalman estimator tracks the step input well. The simulation is also performed with input noise, and the LQG controller effectively attenuates the noise. From the data in Fig. 5(c), it is manifest that the open-loop PEMFC stoichiometry with a large value converges very slowly. The LQG controller controls the oxygen stoichiometry well near the value of 2, but there is a slight deviation from the desired value. This proves that the LQG is not robust. A stack voltage comparison between FF, LQG and TDC is given in Fig. 6. The voltage fluctuation with the LQG controller is larger than those of other controllers because the PEMFC plant for the LQG control is linear; the oxygen stoichiometry fluctuates larger than the others. A larger rate of oxygen mass flow increases the pressure inside the cathode, which causes a larger stack voltage and thereby, increases the parasitic power and decreases the net power. Moreover, the LQG controller shows a sluggish response to reach the other steady-state operating point, which hinders the delivery of immediate power supply in vehicular applications. The LQG controller does not show overshoot, however, because relatively high damping is involved in the controller during the design process of the LQG. As the LQG controller does not regulate oxygen stoichiometry well and has sluggish transient response, only the FF and TDC comparisons are made to discuss the transient response for the PEMFC.

Fig. 7 shows the transient performance of the fuel cell system related to certain steps of the stack current and corresponding variables from the FF and TDC models. It is evident that the discrepancy

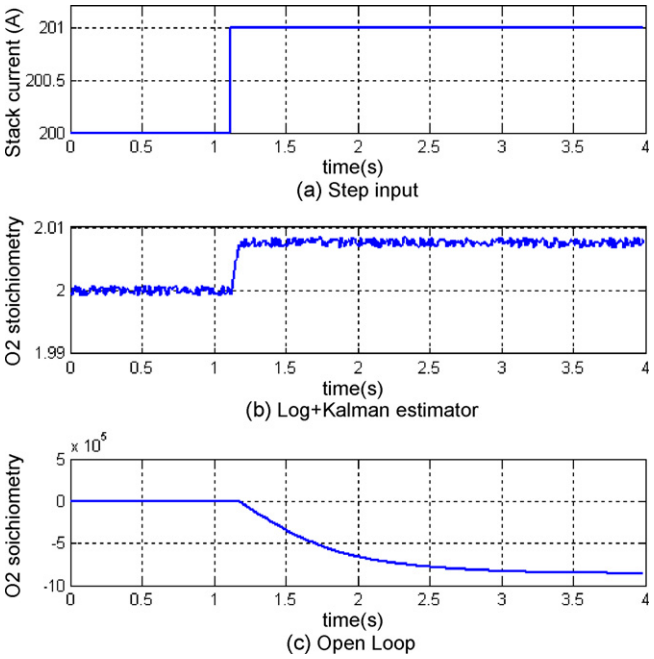

Fig. 5. Comparison between LQG and open-loop system.

between the performances of the FF and TDC models is small. As shown in Fig. 7(a), every step of the stack current lasts for at least 2.5 s, and the electrical load during 17.5–2.5 s is assumed to be the same as that during 12.5–7.5 s. Since the stack current increases, the dynamic response during 0–7.5 s in Fig. 7(b) shows that the air stoichiometric ratio cannot follow this sharp disturbance and decreases instantaneously due to the inertia of the compressor. The increased consumption of oxygen causes the cathode inlet pressure to decrease a little synchronously, as shown in Fig. 7(c). The dynamics of the fuel cell system then transfers gradually to a new steady-state under the updated control inputs. With the step-change of the control input, v_{comp}, the late-increment of the cathode inlet pressure reveals a characteristic of non-minimum phase. This is because both the inlet manifold and compressor inertia exist. If the control input does not correspond to the variation in stack current, a too-sharp increment in the electric load might deplete the oxygen and collapse the fuel cell system. As shown in Fig. 7(b), the FF controller renders the stoichiometry to be approximately 2, but there might be some minor deviation around 2 due to system nonlinearity. FF shows a deeper drop of stoichiometry than TDC and this can cause oxygen starvation. Oxygen stoichiometry also shows

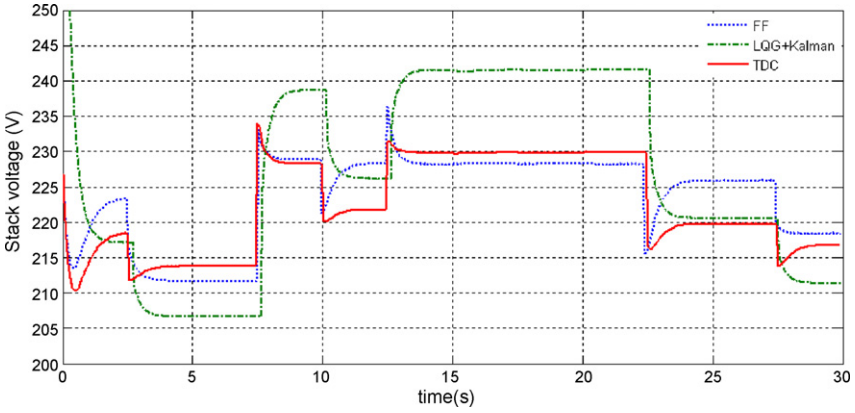

Fig. 6. Comparison of FF, LQG and TDC controller response.

that FF has a sluggish response to the current input because FF has a larger time constant than TDC. Meanwhile, TDC has a fast transient response and the stoichiometry converges to 2 as soon as the transient response vanishes. As the main objective of the PEMFC control is to keep the oxygen stoichiometry to 2 with minimal anode and cathode pressure difference, TDC has better transient performance than FF. For the cathode inlet pressure control, as shown in Fig. 7(c), the FF control shows larger pressure existence inside the cathode than the TDC during 10–30 s. This means that a larger airflow rate is necessary, as shown by the stoichiometry value. As a greater airflow is required, a larger parasitic power loss is engaged, as shown in Fig. 7(d) and (e). The stack voltage output is given in Fig. 7(f) and illustrates that more oxygen is required in the FF control than in TDC.

The transient behaviour of the stack voltage is closely relayed to two physical variables: oxygen stoichiometry and relative humidity [31,32]. As shown in Fig. 7(g), the relative humidity obtained from both control methods is almost the same. The transient char-

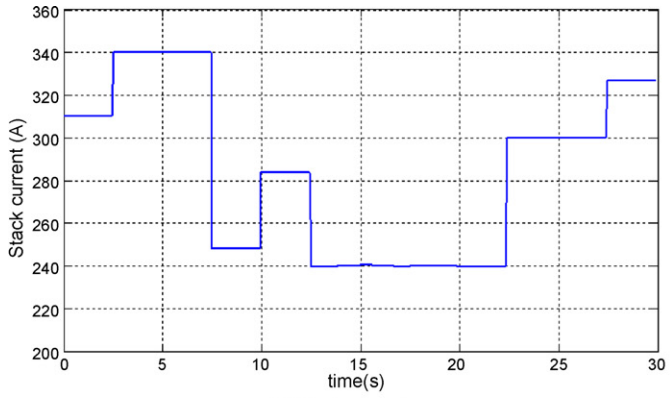

(a) Stack current

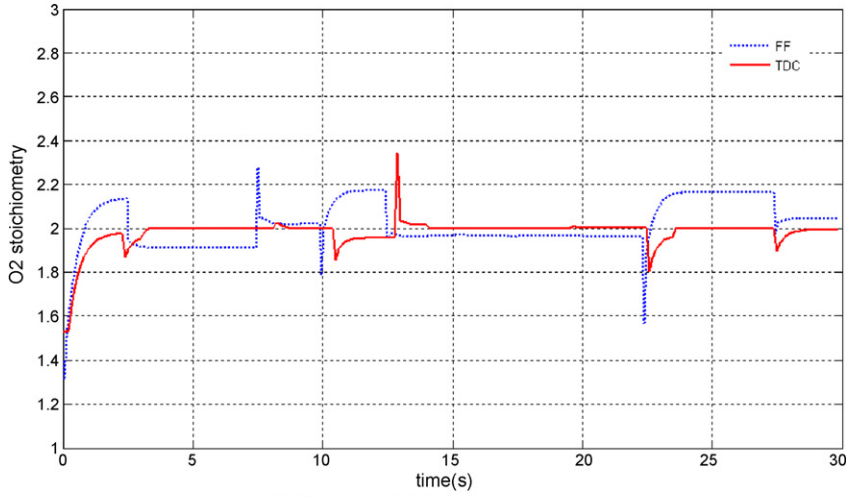

(b) Oxygen stoichiometry

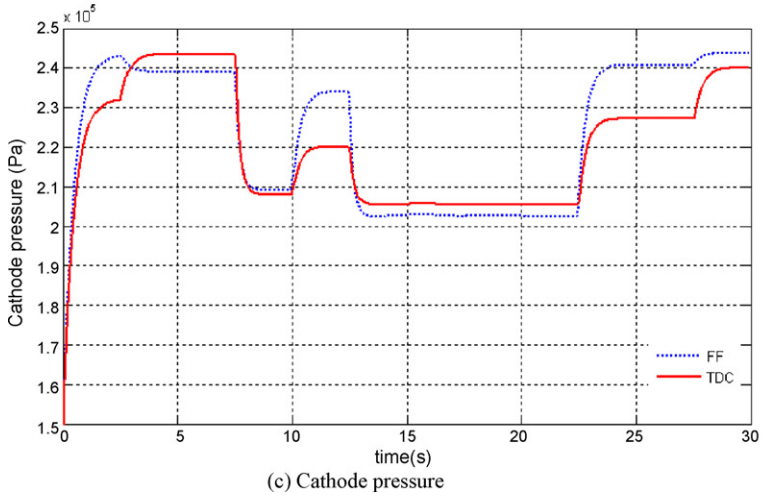

(c) Cathode pressure

Fig. 7. Comparison between FF and TDC for PEM fuel cell variables. (a) Stack current; (b) Oxygen stoichiometry; (c) Cathode pressure; (d) Fuel cell power; (e) Net power; (f) Stack voltage; (g) Cathode relative humidity; (h) Compressor outlet temperature.

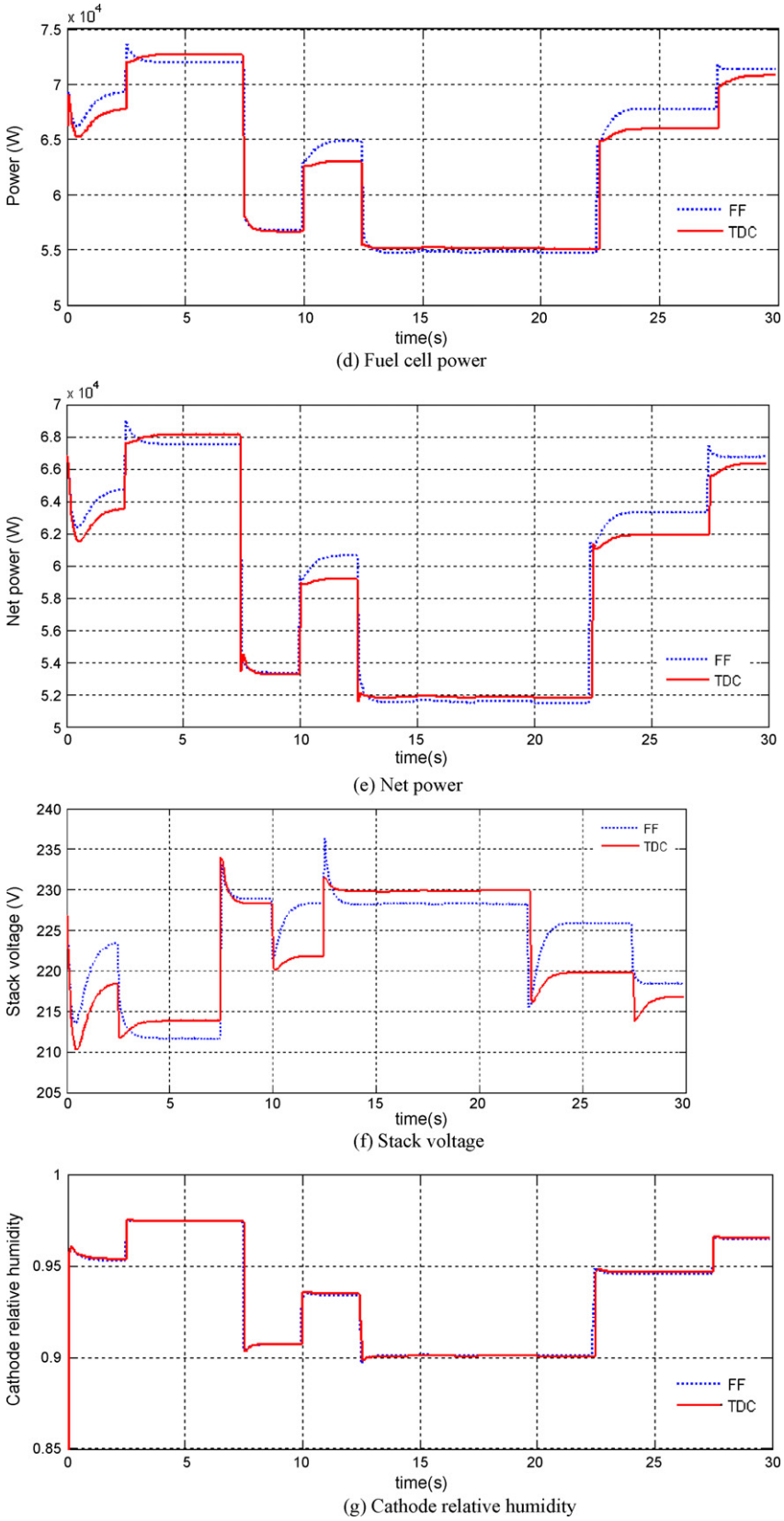

Fig. 7. (*Continued*)

acteristics of the stack voltage is strongly dependent on the oxygen stoichiometry only. In general, when the stack current increases suddenly, the stack voltage has undershoot characteristics and reaches the steady-state after a certain amount time elapses. This amount of time is called the 'time delay'. During this time, due to the supply of humidified gas and internal hydration from the electro-osmotic drag and back diffusion, the membrane becomes hydrated, which results in voltage recovery. Likewise, when the load changes

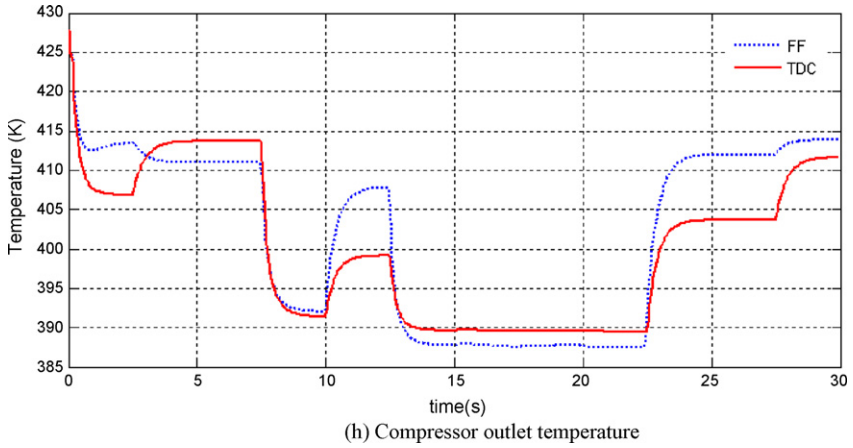

Fig. 7. (*Continued*).

from high to low, the stack voltage shows an overshoot with a time delay. In the simulation, as the stack current increases suddenly from 250 to 285 A at 10 s, as shown in Fig. 7(a), the stack voltage drops instantaneously, as shown in Fig. 7(f). Undershoots are observed from both control actions, but the time delay from FF is a little longer than that of TDC. The steady-state voltage of the FF is also larger than that of the TDC because the oxygen stoichiometry of the FF is larger than that of the TDC. As the time delay is closely related to the air supply speed, TDC shows a slightly better transient behaviour in considering the time delay. Another load increase is engaged at 22.5 s, and the stack voltage variation has the same characteristics as shown at 10 s. The instantaneous stoichiometry, however, drops below 1.6 with the FF control action, as shown in Fig. 9(b). It is reported that if the oxygen stoichiometry is below 1.6, the stack voltage becomes unstable, and it has a longer time delay to reach a steady-state condition [31]. In this sense, the FF control may have an undesirable transient effect in considering a reliable fuel cell operation. Meanwhile, when the load changes from high to low, the stack voltage shows an overshoot. At 12.5 s, the sudden change in stack current occurs from 282 to 240 A. The oxygen stoichiometry of TDC is maintained well at 2, but that of the FF shows a lower one. Both control actions show a voltage overshoot, as shown in Fig. 7(f), but a larger overshoot is detected for FF control. The FF control also shows a longer time delay than that of the TDC control. The steady-state voltage for FF control is also lower than that of the TDC because the oxygen stoichiometry is smaller than the optimum value of 2. Although an ample airflow rate and pressure increase stack voltage and electric power, the excessive compressor parasitic power degrades the net power, as shown in Fig. 7(d) and (e). These represent a trade-off between the stack and the compressor. In net power consumption, neither of the control methods shows a large difference. If the relative humidity is too low, then the membrane dries out and the conductivity decreases. By contrast, if the relative humidity is too high, it produces an accumulation of liquid water on the electrodes, which can flood and block the pores, making gas diffusion difficult [33]. Fig. 7(g) illustrates the relative humidity of the cathode side with a value between 0.9 and 0.97; therefore, the relative humidity is well controlled and thus prevents water flooding or membrane drying using TDC. Fig. 7(h) shows the compressor outlet temperature; since higher oxygen stoichiometry requires more air supply the compressor temperature will increase as expected. FF has more temperature fluctuation than TDC, and a higher temperature (nearly 10 K) is observed in the FF control than in the TDC. It should be noted, however, that both controls need to be cooled to meet the fuel cell operating temperature.

The running trajectory of the compressor related to the same steps of the stack current and the control input in Fig. 7 is demonstrated in Fig. 8. It can be seen that the compressor almost works in the high-efficiency zones. Therefore, there is a good size match between the stack and the compressor.

The anode transient characteristics are presented in Fig. 9. The purge is conducted for 1 s every 5 s interval, as shown in Fig. 9(a), which also gives the purged hydrogen flow rate. Since the purged flow rate depends on the pressure difference between anode and

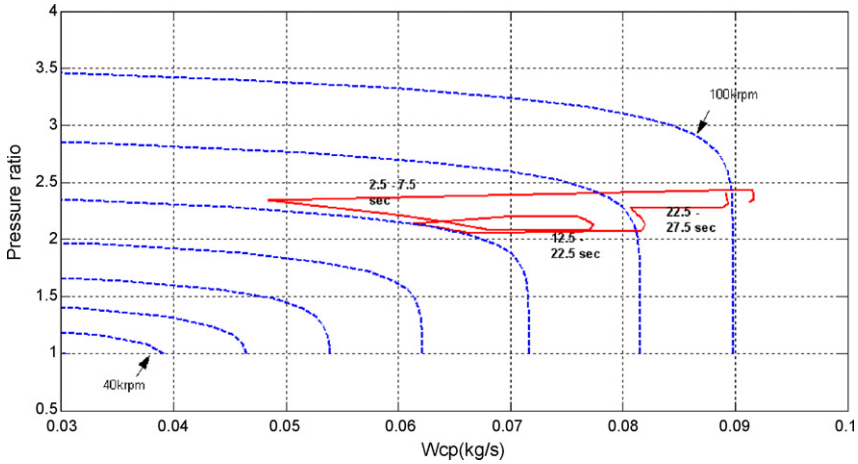

Fig. 8. Compressor map.

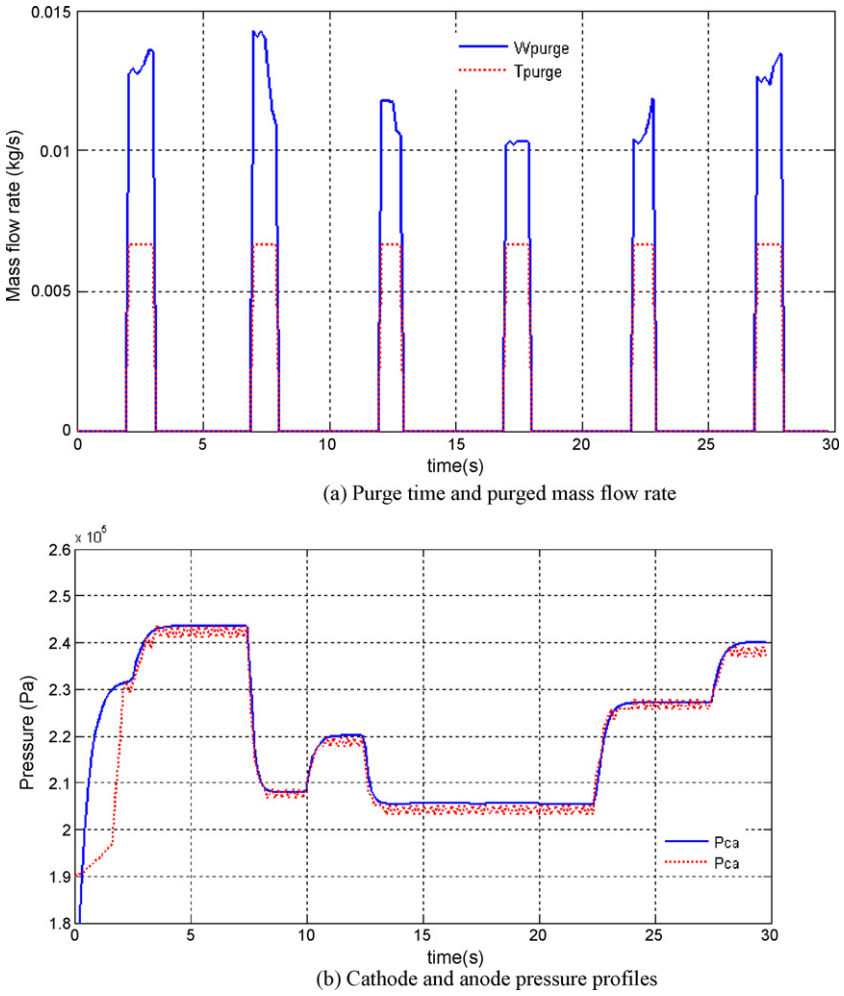

Fig. 9. Anode control. (a) Purge time and purged mass flow rate; (b) Cathode and anode pressure profiles.

atmospheric pressures, the purged flow rate differs at each purge operation. As shown in Fig. 9(b), the anode pressure profile agrees well with the cathode profile with a pressure difference of nearly zero. Given that the hydrogen flow control is intended to minimize the pressure difference across the membrane, TDC performs well to prevent an abrupt pressure gradient difference. Nevertheless, there appear to be minor ripples in the anode pressure because a minor pressure difference always exists between the hydrogen pumping pressure and the inside of the anode pressure. Furthermore, the purging operation instantaneously drops the anode pressure. Analysis shows that the purging effect is not dominant, which agrees with the findings of Bao et al. [17]. If the purging time is longer than 1 s, it shows a larger anode pressure drop. The exact effect of purging time and hydrogen stoichiometry on the anode pressure drop can be taken from Gou et al. [34]. Since the pressure difference between anode and cathode is nearly zero, this proves that the membrane inertial dynamic fluctuation force could be well-maintained to prolong the life of the PEMFC.

5. Conclusions

A PEMFC dynamical model is constructed with a compressor, cooler and humidifier at the cathode, and a hydrogen recirculation injection pump and purging valve at the anode. The compressor input voltage and hydrogen pumping control are selected for the control inputs to improve transient performance, respond quickly to power requirement demands, and prevent oxygen starvation by accurately preserving the desired oxygen stoichiometry as quickly as possible. The objective of the present control is to regulate immediately the oxygen stoichiometry with minimal fluctuation and zero pressure difference between the cathode and the anode. The PEMFC system is highly non-linear with continuous, varying requested power demand in vehicle applications and changing parameters due to temperature variation. A robust control technique is necessary to satisfy these objectives. TDC is chosen and designed to fulfill these objectives satisfactorily. Static FF and LGQ control are also applied in order to prove the effectiveness of TDC in improving transient dynamics. The results show that TDC regulates the oxygen stoichiometry very well with a relatively quick response, and that it minimizes the pressure difference between the anode and the cathode. TDC shows less of a stoichiometry drop than FF, which might prevent oxygen starvation. TDC also gives faster response in oxygen stoichiometry than FF, which is important in supplying immediate power delivery in vehicle applications. Moreover, it provides a well-maintained relative humidity to prevent water flooding or membrane drying. For anode control, it can effectively control anode pressure to allow for a minimum deviation from that at the cathode. In order to minimize the fluctuation of air and fuel pressures further for the sake of stack longevity, other power sources are necessary to alleviate the rapid changes in power demanded from the PEMFC.

Acknowledgement

This research was supported by Basic Science Research Program through the National Research Foundation of Korea (NRF)

funded by the Ministry of Education, Science and Technology (2010-0007213).

References

[1] J.C. Amphlett, R.M. Baumert, R.F. Mann, J. Electrochem. Soc. 142 (1995) 1–15.
[2] D.M. Bernardi, M.W. Verbrugge, J. Electrochem. Soc. 139 (1992) 2477–2491.
[3] T.E. Springer, T.A. Zawodzinski, J. Electrochem. Soc. 138 (1991) 2334–2342.
[4] X. Xue, J. Tang, A. Smirnova, R. England, N. Sammes, J. Power Sources 133 (2004) 188–204.
[5] T.T. Jagaduri, G. Radman, J. Power Sources 77 (2007) 83–92.
[6] S. Piscinger, C. Schonfelder, W. Bornscheuer, SAE Paper (2001) 9–16.
[7] M.D. Lukas, K.Y. Lee, H. Ghezel-Ayagh, IEEE Trans. Energy Convers. 16 (2001) 289–295.
[8] J. Golbert, D.R. Lewin, J. Power Sources 135 (2004) 135–151.
[9] A.J. del Real, A. Arce, C. Bordons, J. Power Sources 173 (2007) 310–324.
[10] P.R. pathapati, X. Xue, J. Tang, Renewable Energy 30 (2005) 1–22.
[11] D.J. Xuan, J.W. Kim, Y.B. Kim, J. Mech. Sci. Technol. 23 (2009) 717–728.
[12] J.T. Pukrushpan, P. Huei, A. Stefanopoulou, J. Dynamic Syst., Measurement Control 126 (2004) 14–25.
[13] J.O. Schumacher, P. Gemmar, M. Denne, M. Zedda, M. Steuber, J. Power Sources 129 (2004) 143–151.
[14] J. Hasikos, H. Sarimveis, P.L. Zervas, M.C. Markatos, J. Power Sources 193 (2009) 258–268.
[15] C. Shen, G. Cao, X. Zhu, X. Sun, J. Process Control 12 (2002) 831–839.
[16] J. Golbert, D.A. Lewin, J. Power Sources 135 (2004) 165–176.
[17] C. Bao, M. Ouyang, Y. Baolian, Int. J. Hydrogen Energy 31 (2006) 1879–1896.
[18] K. Youcef-Toumi, K. Fullbrigge, Proc. IEEE Robotics Automation (1989) 1786–1791.
[19] O. Nejat, S. Rifat, IEEE Automatic Control 47 (2002) 793–797.
[20] D.J. Xuan, J.W. Kim, Y.B. Kim, J. Vibration Control 15 (2009) 1307–1324.
[21] F.C.V. Hyunda's Tucson, Fuel Cells Bull. 5 (2004) 6–7.
[22] S. Choe, J. Lee, J. Ahn, S. Baek, J. Power Sources 164 (2007) 614–623.
[23] M. Ceraolo, C. Miulli, A. Pozio, J. Power Sources 113 (2003) 2178–2186.
[24] T.V. Nguyen, R.E. White, J. Electrochem. Soc. 140 (1993) 2178–2186.
[25] R.F. Mann, J.C. Amphlett, M.A.I. Hooper, H.M. Jensen, B.A. Peppley, P.R. Roberge, J. Power Sources 86 (2000) 173–180.
[26] G. Marsala, P. Marcello, G. Vitale, M. Cirrincione, A. Miraoui, Appl. Energy 86 (2009) 2192–2203.
[27] J.H. Le, T.R. Lalk, J. Power Sources 73 (1998) 229–241.
[28] L.A.M. Riascos, J. Power Sources 184 (2008) 204–211.
[29] O. Nejat, S. Rifat, IEEE Trans. Automatic Control 47 (2002), pp. 793-397.
[30] A. del Real, A. Alicia, C. Bordons, J. Power Sources 173 (2007) 310–324.
[31] J. Cho, H. Kim, K. Min, J. Power Sources 185 (2008) 118–128.
[32] X. Xue, J. Tang, N. Sammes, Y. Ding, J. Power Sources 162 (2006) 388–399.
[33] S.H. Ge, C.Y. Wang, J. Electrochem. Soc. 154 (2007) 998–1005.
[34] J. Gou, O. Pei, Y. Wang, J. Power Sources 162 (2006) 1104–1114.